Infrared Physics & Technology 136 (2024) 105003

Contents lists available at ScienceDirect

Infrared Physics and Technology

journal homepage: www.elsevier.com/locate/infrared

Hybrid nested negative curvature fiber with ultra-low-loss in the terahertz band

Qiang Liu [a,b], Guangrong Sun [a,b], Haiwei Mu [a,b], Wei Liu [a,b], Tingting Lv [a,b], Chao Ma [a,b], Wenjing Li [a,b], Kaiyu Wang [a,b], Jingwei Lv [a,b], Paul K. Chu [c], Chao Liu [a,b,*]

[a] School of Physics and Electronic Engineering, Northeast Petroleum University, Daqing 163318, China
[b] SANYA Offshore Oil & Gas Research Institute, Northeast Petroleum University, Sanya 572024, China
[c] Department of Physics, Department of Materials Science and Engineering, and Department of Biomedical Engineering, City University of Hong Kong, Tat Chee Avenue, Kowloon, Hong Kong, China

ARTICLE INFO

Keywords:
Hybrid nested negative curvature fiber
Three-layer anti-resonant effect
High-resistivity silicon
Dielectric layers

ABSTRACT

A novel hybrid nested negative curvature fiber (NCF) based on the three-layer anti-resonant effect is described. The elliptical tubes cladding structure exhibits the advantage of flexible design and can effectively reduce propagation losses. The influences of the nested methods and structural parameters on the propagation characteristic are analyzed numerically. Since high-resistance silicon (HRS) has an ultra-low absorption coefficient in the THz frequency range, the effective material loss is reduced. Meanwhile, the three-layer nested structure suppresses the confinement loss, the total loss is as low as 6.62×10^{-5} dB/m at 1.1 THz. The effects of the number of cladding tubes and dielectric layers on the propagation loss are compared and analyzed. The optimized NCF shows a loss of less than 10^{-4} dB/m between 1 and 1.06 THz and 1.1–1.24 THz. The result reveals a new method to design broadband ultra-low-loss hollow-core NCFs.

1. Introduction

In order to meet the needs of optical imaging [1], quantum-cascade lasers [2], chemical reaction monitoring [3], biomedical sensing [4], DNA genetic diagnostics [5], and 6G wireless communication [6] in the terahertz band, various terahertz waveguides such as metal waveguides and dielectric waveguides have been proposed [7]. Metal waveguides are prone to high ohmic and propagation losses [8], while dielectric waveguides have significant advantages such as propagation losses enabling low-loss and low-dispersion terahertz wave propagation. Especially, hollow-core fibers (HCFs) have attracted attention due to their low nonlinearity, low dispersion, low material absorption, high damage threshold, and low propagation delay [9]. Such remarkable optical properties exhibit great application potential in high-power delivery, high-speed data communication and ultra-short pulse delivery [10].

HCFs are mainly divided into photonic bandgap fibers [11] (PBGFs) and negative curvature fibers [12] (NCFs). PBGFs use the photonic bandgap effect to limit the mode in the core region, and the propagation loss can be reduced by increasing the number of cladding layers. However, due to the bandgap effect, the low-loss bandwidth of PBGFs is relatively narrow [13]. NCFs are based on the anti-resonant effect which can suppress the coupling between the core modes and cladding modes to achieve broadband low-loss propagation by adjusting the structure of the cladding tubes to control the resonant wavelength or frequency [14]. Previous studies have shown that the propagation loss of NCFs is influenced by the size of the core, number of dielectric layers, wall thickness of the cladding tubes, number of cladding tubes, distance between adjacent tubes, and shape of the cladding tubes [15–18]. Currently, there are various designs such as tubular structures including circular, elliptical, ice cream shaped single-layer tubes [19–21] and nested tubes [22–24]. In particular, NCFs based on elliptical tubes cladding structure have attracted attention due to their flexible curvature and design freedom in performance optimization. In the infrared band, S. Gao et al. [12] have designed and fabricated a NCF based on conjoined tubes with a propagation loss of 0.02 dB/m at 1,512 nm. F. Amrani et al. [25] have reported and fabricated a NCF with a hybrid cladding structure composed of Kagome tubes and single-layer circular tubes with a propagation loss of 0.016 dB/m at 1,050 nm. Y. Yu et al. [20] have numerically analyzed a NCF consisting of single-layer

* Corresponding author at: School of Physics and Electronic Engineering, Northeast Petroleum University, Daqing 163318, China.
E-mail address: nepulq@126.com (C. Liu).

https://doi.org/10.1016/j.infrared.2023.105003
Received 5 September 2023; Received in revised form 11 November 2023; Accepted 20 November 2023
Available online 23 November 2023

elliptical tubes and optimized the fiber performance by changing the positive and negative ellipticity of the elliptical tubes, resulting in a propagation loss of 10^{-4} dB/m at 1,550 nm. J. Zhang et al. [10] have proposed a NCF composed of three-layer nested structure showing a propagation loss of 6.45×10^{-9} dB/m at 1,060 nm. However, the reported NCFs exhibit relatively high propagation loss in the terahertz band.

Therefore, researchers have attempted to utilize different materials and novel structures to design low-loss THz NCFs. M. M. Nazarov et al. [26] have numerically analyzed and developed a THz NCF using PP based on single-layer circular tubes showing a propagation loss of 3.8 dB/m at 2.15 THz. S. Yang et al. [27] have designed and fabricated a THz NCF comprising single-layer semi-elliptical tubes with a propagation loss of 1.26 dB/m at 0.82 THz. W. Talataissong et al. [28] have proposed and fabricated a THz NCF based on hexagonal tubes constructed with Topas and the propagation loss is 12 dB/m at 0.7 THz. J. Sultana et al. [29] have studied three types of THz NCFs using Zeonex and compared the performance of non-nested circular tubes, nested circular tubes, and adjacent nested circular tubes. The propagation loss of the optimal structure is 0.055 dB/m at 1 THz. The previously reported THz NCFs are all based on single-layer or double-layer anti-resonant effect and are difficult to further reduce propagation loss.

In this paper, we describe a novel hybrid nested negative curvature fiber (HN-NCF) based on three-layer anti-resonant effect. The cladding is constructed with elliptical tubes, the nested straight bars and circular tubes, which form the nodeless cladding structure to reduce the confinement loss of HN-NCF. At the same time, the HRS material reduces the effective material loss giving rise to excellent characteristics. The effects of the number of cladding tubes and dielectric layers on the propagation properties of HN-NCF are analyzed and compared. Our results show that the NCF with the six three-layer hybrid nested cladding structure delivers the best performance.

2. Fiber design

Fig. 1 presents the three HN-NCFs, with the green and white areas being the HRS material and air, respectively. The figure is divided into three parts by the dash dot line corresponding to the local cladding structures of the three types of NCFs. The outer cladding tubes have a nodeless elliptical shape and the inner cladding tubes contain a straight bar and circular tubes with various nested position. Structure (1) nests the circular tubes inside the elliptical tubes near the jacket tube (HN-NCF1), structure (2) nests the circular tubes near the core (HN-NCF2), and structure (3) adopts the simultaneous nested circular tubes structure (HN-NCF3). The nodeless cladding structures are adopted to reduce

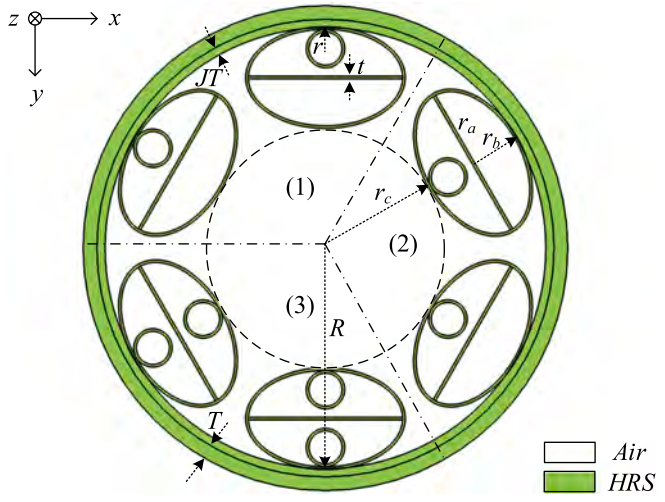

Fig. 1. Cross-section of the three HN-NCFs.

additional resonance caused by multiple nodes [26]. The core radius r_c is 4.3 mm, and the semi-major axis and semi-minor axis of the outer elliptical tubes are $r_a = 2.9$ mm and $r_b = 1.85$ mm, respectively. The nested straight bars overlap the major axis of the elliptical tubes, and the radius of the nested circular tubes is $r = 0.8$ mm. The wall thickness t of the cladding tubes is 0.03 mm. The thicknesses of the jacket tube and the perfectly matched layer are $JT = 0.3$ mm and $T = 0.5$ mm, respectively. The fiber inner radius R is 8 mm.

3. Results and discussion

The characteristics of the NCF are analyzed by the full-vector finite element method. In order to ensure the accuracy of the numerical calculations, the HRS material and air hole are divided into extremely fine mesh sizes of $\lambda/6$ and $\lambda/4$, respectively. As for the tubular NCFs, the low-loss region is between two adjacent resonant frequencies. The resonant frequency can be calculated by Eq. (1) [30,31]:

$$f_c = \frac{mc}{2t\sqrt{n^2-1}} \tag{1}$$

where c is the velocity of light in vacuum, m is the order of resonance, n is the refractive index of the HRS material which is set to be a constant of 3.417 in the 0.5–4.5 THz range [32] and t is the wall thickness of the cladding tubes.

The confinement loss and effective material loss of THz NCF can be calculated using the following Eq. (2) and Eq. (3) [33,34]:

$$CL = 8.686\left(\frac{2\pi f}{c}\right) Im\left(n_{eff}\right), [dB/m] \tag{2}$$

$$EML = 4.34\sqrt{\frac{\varepsilon_0}{\mu_0}}\frac{\int_{A_{mat}} n\alpha_{mat}|E|^2 dA}{2\int_{All} S_z dA}, [dB/m] \tag{3}$$

where f is the operating frequency, $Im(n_{eff})$ is the imaginary part of the effective refractive index, ε_0 and μ_0 are the permittivity and permeability in vacuum, respectively, α_{mat} is the material absorption coefficient of HRS which is approximately 1 m^{-1} around 1.1 THz [33], and S_z is the Poynting vector along the z-direction.

3.1. Propagation loss

When $R = 8$ mm, $JT = 0.3$ mm, $t = 0.03$ mm, $r = 0.8$ mm, $r_a = 2.9$ mm, $r_b = 1.85$ mm and $r_c = 4.3$ mm, the loss spectra of the three HN-NCFs are studied, as shown in Fig. 2. Fig. 2(a) shows that the confinement loss of HN-NCF1 is significantly lower than those of HN-NCF2 and HN-NCF3 in the range of 0.6–1.6 THz and the low-loss bandwidth is wider. The minimum confinement loss occurs at 1.14 THz and it is only 1.84×10^{-5} dB/m. The confinement losses of HN-NCF2 and HN-NCF3 are greater, because the wall thickness of the core-cladding boundary is equivalent to the superposition of the two wall thicknesses, that is, the equivalent wall thickness t being 0.06 mm. According to Eq. (1), there is resonance at 0.76 THz. Fig. 2(b) shows the effective material loss spectra of the three HN-NCFs. The effective material loss of HN-NCF1 changes smoothly, but those of HN-NCF2 and HN-NCF3 fluctuate significantly due to two resonances in this spectral range. The total loss is obtained by superposing the confinement loss and effective material loss, as shown in Fig. 2(c). The smallest total loss is only 6.62×10^{-5} dB/m for HN-NCF1. At the same time, the low-loss bandwidth below 10^{-3} dB/m is the widest and up to 0.54 THz. The frequency range below 10^{-4} dB/m also reaches 0.2 THz. Fig. 2(d) shows the electric field contour diagrams of the three HN-NCFs at typical frequencies, and the corresponding total loss values are shown below the block diagrams. The two black block diagrams present the electric field contour diagrams of HN-NCF1 at 1 THz (left) and 1.1 THz (right), indicating that the electric field is well controlled in the core region. The red and blue block diagrams show the

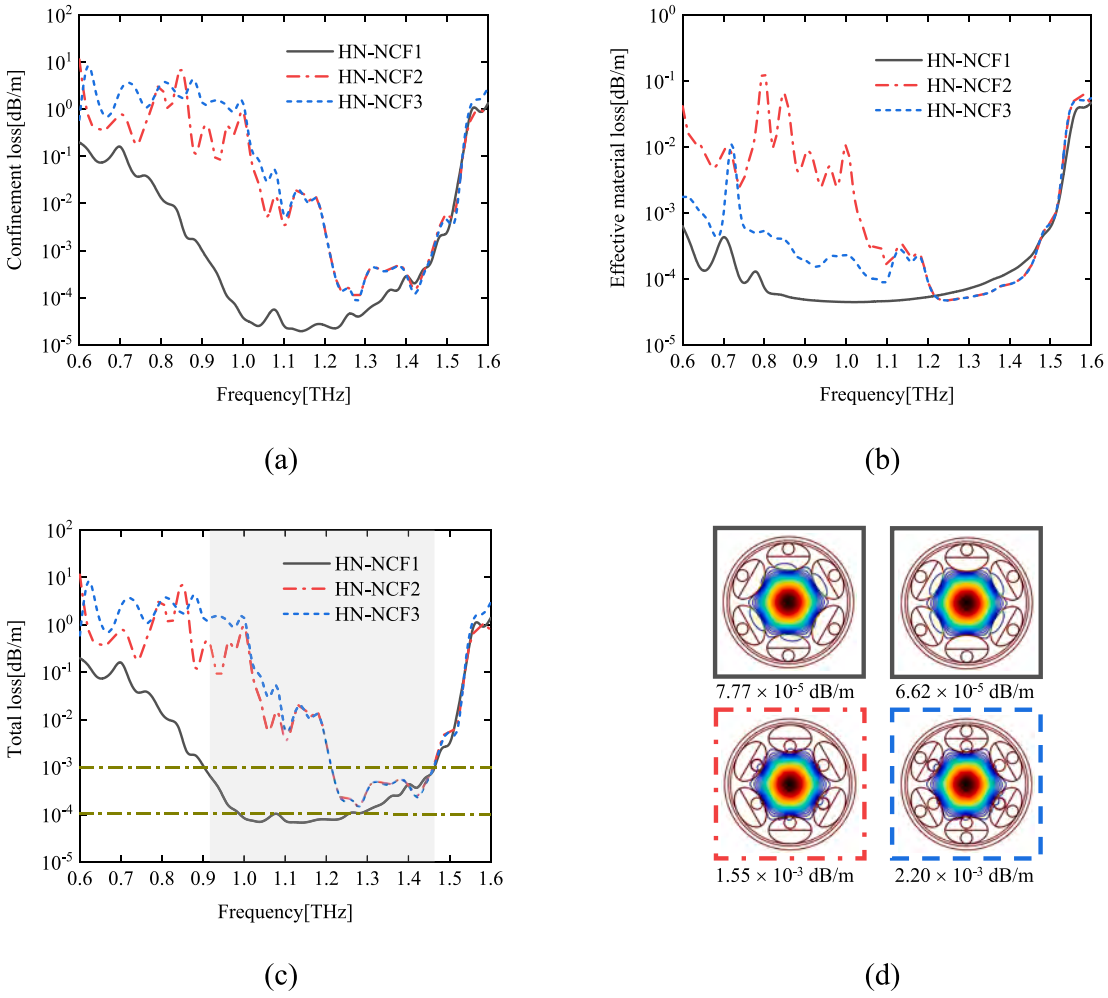

Fig. 2. Propagation properties of the three HN-NCFs: (a) Confinement loss, (b) Effective material loss, (c) Total loss and (d) Electric field contour diagrams at typical frequencies.

electric field contour diagrams of HN-NCF2 and HN-NCF3 at 1.1 THz, respectively. The electric field shows leakage, indicating that the circular tubes near the core have a significant impact on the total loss. Therefore, HN-NCF1 is the optimal structure and 1.1 THz is selected to be the working frequency in the following discussion.

3.2. Parametric optimization

When $R = 8$ mm, $JT = 0.3$ mm, $t = 0.03$ mm, $r = 0.8$ mm, $r_b = 1.85$ mm and $r_c = 4.3$ mm, the influence of the semi-major axis r_a of the elliptical tubes of HN-NCF1 on the total loss spectra is shown in Fig. 3(a). When $r_a = 2.2$ mm, the minimum total loss is 3.38×10^{-4} dB/m. As the

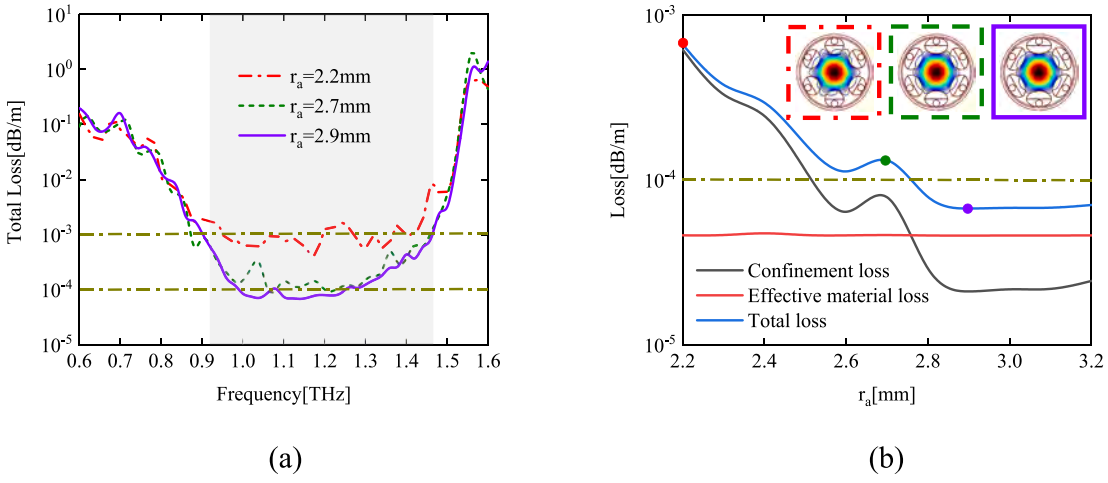

Fig. 3. Influence of the semi-major axis r_a on loss: (a) Total loss versus frequencies and (b) Loss for various semi-major axes at 1.1 THz.

semi-major axis r_a increases, the total loss decreases gradually. The HN-NCF1 has lower total loss and wider low-loss bandwidth for $r_a = 2.9$ mm. In order to analyze the impact of r_a on the propagation loss, the losses for various semi-major axes at 1.1 THz are shown in Fig. 3(b). As r_a changes from 2.2 mm to 3.2 mm, the effective material loss changes smoothly, the confinement loss and total loss both decrease and then flatten. This is because when the semi-major axis r_a is larger, the distance between the outer elliptical tubes is smaller. The electric field is difficult to leak through the gap resulting in a smaller total loss. The block diagram in Fig. 3(b) shows the electric field contour diagrams for various semi-major axes. The leakage of the electric field is most significant as $r_a =$ 2.2 mm (red block diagram), while the electric fields in the green block diagram ($r_a = 2.7$ mm) and purple block diagram ($r_a = 2.9$ mm) are better limited in the core region. The total loss reaches a minimum as r_a = 2.9 mm and therefore, it is selected to be the optimal value in the following analysis.

When $R = 8$ mm, $JT = 0.3$ mm, $t = 0.03$ mm, $r = 0.8$ mm and $r_a = 2.9$ mm, the influence of the semi-minor axis r_b of the elliptical tubes of HN-NCF1 on the total loss spectra is shown in Fig. 4(a). When the semi-minor axis is smaller ($r_b = 1.7$ mm), the total loss is larger and the minimum is 7.95×10^{-5} dB/m. As the semi-minor axis r_b increases, the low-loss bandwidth widens, and the lowest total loss decreases gradually and then increases. When $r_b = 1.85$ mm, the frequency range lower than 10^{-4} dB/m is the widest. However, the total loss is higher than $r_b = 2.2$ mm due to the additional resonance caused by the small distance between the straight bars and circular tubes at low frequencies. In order to determine the optimal r_b, the losses for various semi-minor axes at 1.1 THz are shown in Fig. 4(b). As r_b changes from 1.7 mm to 2.2 mm, the effective material loss increases tardily. The confinement loss decreases initially and then becomes flat. Therefore, the total loss decreases speedily and then increases tardily. The electric field contour diagrams in Fig. 4(b) reflect the leakage of the electric field for various semi-minor axes. When $r_b = 1.7$ mm (red diagram) and $r_b = 2.2$ mm (purple diagram), the electric field generates a smaller leakage and the loss is larger. When $r_b = 1.85$ mm (green diagram), the electric field is better limited in the core region, and the total loss is the smallest. Considering the frequency range below 10^{-4} dB/m and minimum loss, $r_b = 1.85$ mm is chosen to be the optimal value.

When $R = 8$ mm, $JT = 0.3$ mm, $t = 0.03$ mm, $r_a = 2.9$ mm, $r_b = 1.85$ mm and $r_c = 4.3$ mm, the influence of the radius r of the circular tubes of HN-NCF1 on the total loss spectra is shown in Fig. 5(a). When the radius r is 0.9 mm, the total loss in the range of 0.6–1.6 THz is larger, and the low-loss bandwidth is narrower. This is because a larger radius causes additional resonance when the straight bars and circular tubes are too close together. As the radius r decreases to 0.8 mm, the additional resonant effect weakens, the low-loss bandwidth increases, and the lowest total loss decreases gradually and then increases. When the radius r continues to decrease, the third-layer anti-resonant effect weakens, leading to an increase in the minimum loss. The losses for various radii at 1.1 THz are shown in Fig. 5(b). As r changes from 0.4 mm to 0.9 mm, the effective material loss remains basically unchanged, and the confinement loss and total loss decrease tardily at first and then increase speedily. In order to obtain the lowest propagation loss, $r = 0.8$ mm is chosen to be the optimal value.

3.3. Influence of numbers of cladding tubes

Fig. 6(a) shows the total loss spectra corresponding to the number of cladding tubes including three, four, five, and six cladding tubes. Fig. 6 (b) shows the electric field contour diagrams at 1.1 THz. The fewer the number of cladding tubes, the greater the distance between the adjacent tubes and the electric field can leak more easily from the gaps, resulting in a greater total loss. At 1.1 THz, the corresponding losses for the four structures are 1.21×10^{-1} dB/m, 1.70×10^{-2} dB/m, 5.42×10^{-4} dB/m and 6.62×10^{-5} dB/m. As the number of cladding tubes increases, the electric field can be better limited in the core region and so the six-tube structure is chosen to be the optimal structure.

3.4. Influence of numbers of dielectric layers

In order to analyze the influence of each dielectric layer on the propagation properties, the total loss spectra and electric field contour diagrams at 1.1 THz are calculated for the four cases: non-nested structure, single-layer nested straight bars structure, single-layer nested circular tubes structure, and hybrid nested structure, as shown in Fig. 7(a) and (b). The electric field of red dash dot line corresponds to the non-nested structure and exhibits obvious leakage. The total loss is 2.68 $\times 10^{-3}$ dB/m at 1.1 THz. It is because the single dielectric layer structure has only the one-layer anti-resonant effect. The structures of nested straight bars and nested circular tubes have dual dielectric layers, which greatly enhance the anti-resonant effect and ensure better confinement of the electric field. As shown in the blue and green block diagrams of Fig. 7(b), the losses are 1.96×10^{-4} dB/m and 1.10×10^{-4} dB/m at 1.1 THz, respectively. The hybrid nested structure has three dielectric layers which can greatly reduce propagation losses in this frequency range. It has a wide low-loss bandwidth and the minimum loss reaches 6.62×10^{-5} dB/m. The novel structure opens up a new method for the design of low-loss propagation waveguides in the terahertz band.

4. Conclusion

A novel HC-NCF based on a three-layer nested structure is designed

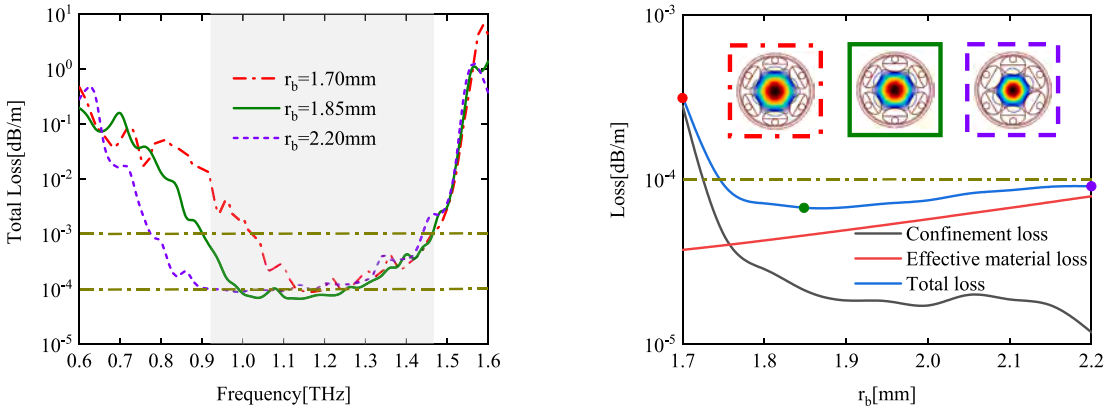

Fig. 4. Influence of the semi-minor axis r_b on loss: (a) Total loss versus frequencies and (b) Loss for various semi-minor axes at 1.1 THz.

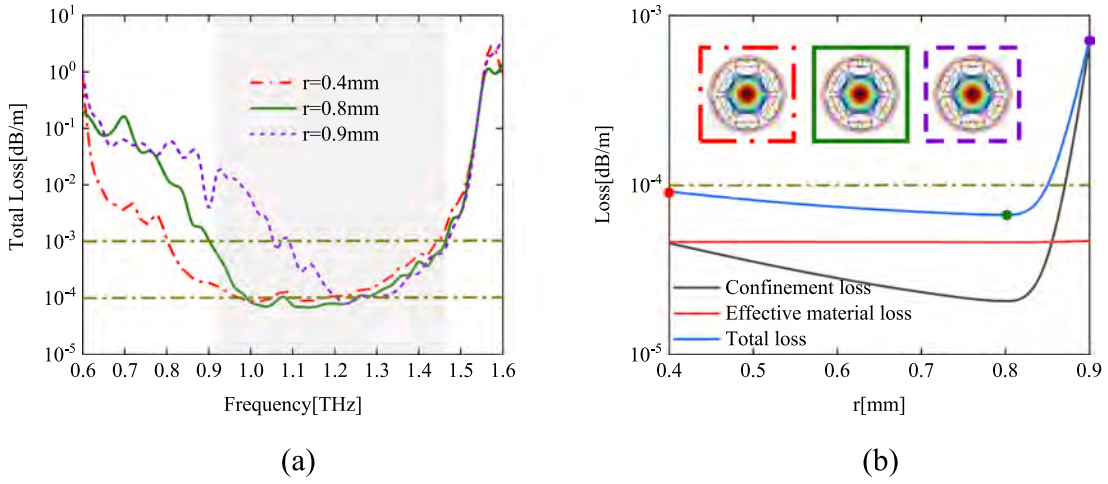

Fig. 5. Influence of the radius *r* on loss: (a) Total loss versus frequencies and (b) Loss for various radii at 1.1 THz.

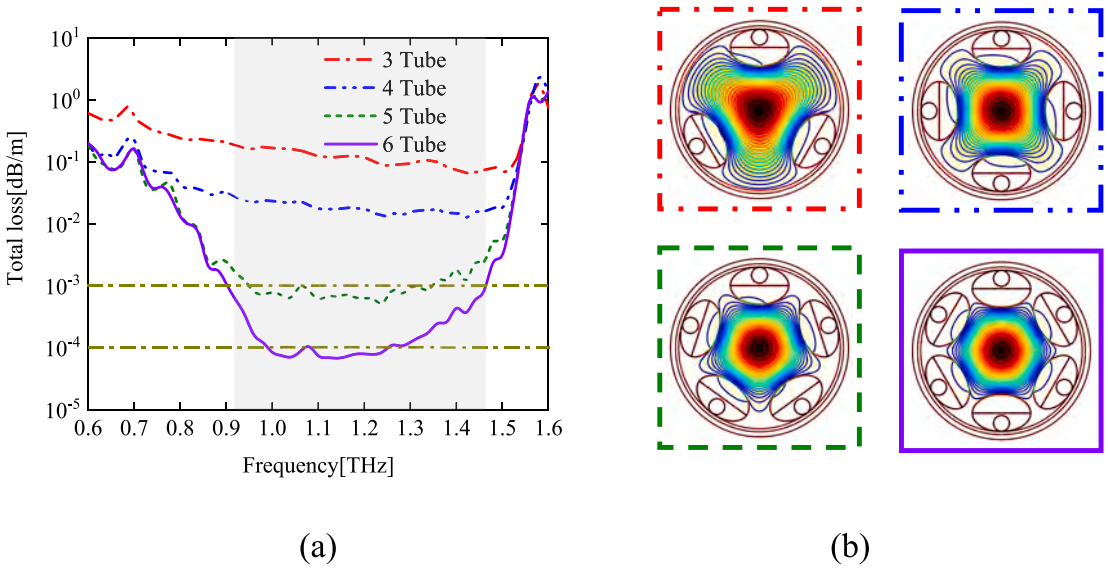

Fig. 6. (a) Total loss versus frequencies for various numbers of cladding tubes and (b) Electric field contour diagrams at 1.1 THz.

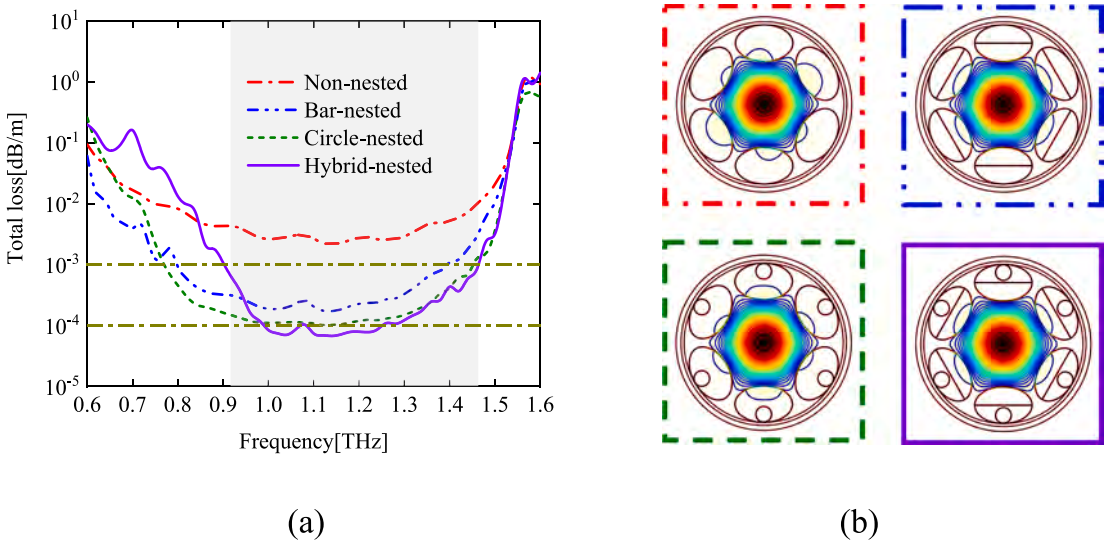

Fig. 7. (a) Total loss versus frequencies for various numbers of dielectric layers and (b) Electric field contour diagrams at 1.1 THz.

and analyzed numerically to determine the effects of the nested positions, number of cladding tubes, dielectric layers, and structural parameters on the propagation properties of the fiber. The results show that compared with non-nested structure, single-layer nested straight bars structure and single-layer nested circular tubes structure, the three-layer hybrid nested structure can better suppress the confinement loss and exhibits a wider low-loss bandwidth. Meanwhile, the HRS with an ultra-low absorption coefficient suppresses effective material loss. The confinement loss and effective material loss are as low as 2.02×10^{-5} dB/m and 4.6×10^{-5} dB/m at 1.1 THz, respectively. The total loss is only 6.62×10^{-5} dB/m and the low-loss bandwidth ($<10^{-3}$ dB/m) reaches 0.54 THz. The performance is significantly superior to the previously reported THz NCFs. This work provides a new scheme for designing low-loss THz NCFs.

Declaration of Competing Interest

The authors declare that they have no known competing financial interests or personal relationships that could have appeared to influence the work reported in this paper.

Data availability

The data that has been used is confidential.

Acknowledgements

This work was jointly supported by Basic Research Support Project for the Excellent Youth Scholars of Heilongjiang Province, Hainan Province Science and Technology Special Fund [ZDYF2022GXJS003], the Provincial Talent Project [ts26180221], Local Universities Reformation and Development Personnel Training Supporting Project from Central Authorities, Natural Science Foundation of Heilongjiang Province [grant number LH2021F007], China Postdoctoral Science Foundation funded project [grant number 2020 M670881], City University of Hong Kong Strategic Research Grant (SRG) [grant number 7005505], City University of Hong Kong Donation Research Grant [grant number DON-RMG 9229021].

References

[1] T. Gretzinger, K. Radhanpura, P. Fairman, M. Berman, D. Farrant, Terahertz reflection hyperspectral 3D imaging using beam scanning, Opt. Exp. 31 (9) (2023) 13998–14007.
[2] H. Bai, G. Liu, K. Wang, G. Chang, S. Zang, C. Tan, L. Gan, Y. Zhang, L. He, G. Xu, Continuous-wave terahertz quantum cascade microlaser arrays operating on various bound states in the continuum, Opt. Express 31 (17) (2023) 27914–27926.
[3] W. Ouyang, C. Ding, Q. Liu, Q. Lu, Z. Wu, Influence analysis of uncertainty of chemical reaction rate under different reentry heights on the plasma sheath and terahertz transmission characteristics, Results. Phys 53 (2023), 106983.
[4] P. Zamzam, P. Rezaei, Y.I. Abdulkarim, O.M. Daraei, Graphene-based polarization-insensitive metamaterials with perfect absorption for terahertz biosensing applications: analytical approach, Opt. Laser Technol 163 (2023), 109444.
[5] H. Cheon, J.K. Hur, W. Hwang, H. Yang, J. Son, Epigenetic modification of gene expression in cancer cells by terahertz demethylation, Sci. Rep 13 (2023) 4930.
[6] H. Zhang, N. Shlezinger, F. Guidi, D. Dardari, Y.C. Eldar, 6G wireless communications: from far-field beam steering to near-field beam focusing, IEEE Commun. Mag 61 (4) (2023) 22963170.
[7] Z. Du, Y. Zhou, S. Luo, Y. Zhang, J. Shao, Z. Guan, H. Yang, D. Chen, Highly birefringent hollow-core anti-resonant terahertz fiber with a thin strut microstructure, Opt. Express 30 (3) (2023) 3783–3792.
[8] S. Islam, J. Sultana, A. Dinovitser, B.W.H. Ng, D. Abbott, A novel Zeonex based oligoporous-core photonic crystal fiber for polarization preserving terahertz applications, Opt. Commun 413 (2018) 242–248.
[9] D. Wu, F. Yu, Y. Liu, M. Liao, Dependence of waveguide properties of anti-resonant hollow-core fiber on refractive index of cladding material, J. Lightwave Technol 37 (21) (2019) 5593–5599.
[10] J. Zhang, J. Cao, B. Yang, X. Liu, Y. Cheng, C. Bao, S. Xie, L. Dong, Q. Hao, Ultralow loss hollow-core negative curvature fibers with nested elliptical antiresonance tubes, Opt. Express 30 (10) (2022) 17437–17450.
[11] Y. Wang, C. Gong, X. Yang, T. Zhu, K. Zhang, Y. Rao, L. Wei, Y. Gong, Photonic Bandgap Fiber Microlaser with Dual-Band Emission for Integrated Optical Tagging and Sensing, Laser Photonics Rev 17 (2023) 2200834.
[12] S. Gao, Y. Wang, W. Ding, D. Jiang, S. Gu, X. Zhang, P. Wang, Hollow-core conjoined-tube negative-curvature fibre with ultralow loss, Nat. Commun 9 (1) (2018) 2828.
[13] A. Mollah, S. Rana, H. Subbaraman, Polarization filter realization using low-loss hollow-core anti-resonant fiber in THz regime, Results. Phys 17 (2020), 103092.
[14] F. Poletti, Nested antiresonant nodeless hollow core fiber, Opt. Express 22 (20) (2014) 23807–23828.
[15] C. Wei, R.J. Weiblen, C.R. Menyuk, J. Hu, Negative curvature fibers, Adv. Opt. Photonics 9 (3) (2017) 504–561.
[16] W. Ding, Y. Wang, S. Gao, M. Wang, P. Wang, Recent progress in low-loss hollow-core anti-resonant fibers and their applications, IEEE J. Sel. Top. Quantum Electron 26 (4) (2020) 4400312.
[17] D. Bird, Attenuation of model hollow-core, anti-resonant fibres, Opt. Express 25 (19) (2017) 23215–23237.
[18] Y. Wang, W. Ding, Confinement loss in hollow-core negative curvature fiber: a multi-layered model, Opt. Express 25 (26) (2017) 33122–33133.
[19] D. Wu, F. Yu, M. Liao, Understanding the material loss of anti-resonant hollow-core fibers, Opt. Express 28 (8) (2020) 11840.
[20] Y. Yu, X. Zhang, Q. Zhang, K. Wang, Y. Yang, Z. Wang, Y. Wang, Y. Huang, J. Wen, W. Chen, T. Wang, Parametric optimization for low loss negative curvature hollow core fiber with elliptical tube, J. Lightwave Technol 41 (1) (2023) 293–300.
[21] A. Deng, I. Hasan, Y. Wang, W. Chang, Analyzing mode index mismatch and field overlap for light guidance in negative-curvature fibers, Opt. Express 28 (19) (2020) 27974–27988.
[22] S. Habib, J.E.A. Lopez, C. Markos, A. Schulzgen, R.A. Correa, Single-mode, low loss hollow-core anti-resonant fiber designs, Opt. Express 29 (8) (2019) 3824–3836.
[23] F. Meng, B. Liu, Y. Li, C. Wang, M. Hu, Low loss hollow-core antiresonant fiber with nested elliptical cladding elements, IEEE Photonics J 9 (1) (2017) 7100211.
[24] X. Zhao, X. Wu, X. Lan, J. Luo, L. Zhang, P. Li, J. Xiang, W. Ma, S. Wang, 5-tube hollow-core anti-resonant fiber with ultralow loss and single mode, Opt. Commun 501 (2021), 127347.
[25] F. Amrani, J.H. OsoRio, F. Delahaye, F. Giovanardi, L. Vincetti, B. Debord, F. Gerome, F. Benabid, "Low-loss single-mode hybrid-lattice hollow-core photonic-crystal fibre", Light: Sci, Appl 10 (2021) 7.
[26] M.M. Nazarov, A.V. Shilov, K.A. Bzheumikhov, Z.C. Margushev, V.I. Sokolov, A. B. Sotsky, A.P. Shkurinov, Eight-capillary cladding THz waveguide with low propagation losses and dispersion, IEEE Trans. Terahertz Sci. Technol 8 (2) (2018) 183–191.
[27] S. ang, X. Sheng, G. Zhao, S. Lou, and J. Guo, "3D printed effective single-mode terahertz antiresonant hollow core fiber", IEEE Access 9 2021 29599 29608.
[28] W. Talataisong J. Gorecki L.D.V. Putten R. smaeel, J. Williamson, K. Addinall, D. Schwendemann, M. Beresna, V. Apostolopoulos, and G. Brambilla, Hollow-core antiresonant terahertz fiber-based Topas extruded from a 3D printer using a metal 3D printed nozzle Photonics Res 9 8 2021 1513 1521.
[29] J. Sultana, S. Islam, C.M.B. Cordeiro, S. Habib, A. Dinovitser, B.W. Ng, D. Abbott, Exploring low loss and single mode in antiresonant tube lattice terahertz fibers, IEEE Access 8 (2020) 113309–113317.
[30] G.K.M. Hasanuzzaman, S. Iezekie, C. Markos, S. Habib, Hollow-core fiber with nested anti-resonant tubes for low-loss THz guidance, Opt. Commun 426 (2018) 477–482.
[31] G. Sun, Q. Liu, H. Mu, Y. Sun, S. Wang, M. Han, J. Wang, J. Lv, P.K. Chu, C. Liu, Anti-resonant fiber with nested U-shape tubes for low-loss terahertz waveguides, Opt. Laser Technol 163 (2023), 109424.
[32] J. Dai, J. Zhang, W. Zhang, W. Zhang, D. Grischkowsky, Terahertz time-domain spectroscopy characterization of the far-infrared absorption and index of refraction of high-resistivity, float-zone silicon, J. Opt. Soc. Am. B 21 (7) (2004) 1379–1386.
[33] A. Mollah, S. Habib, S. Habib, Novel hollow-core asymmetric conjoined-tube anti-resonant fiber for low-loss THz wave guidance, OSA Continuum 3 (5) (2020) 1169–1176.
[34] I.M. Ankan, A. Mollah, J. Sultana, S. Islam, Negative curvature hollow-core anti-resonant fiber for terahertz sensing, Appl. Opt 59 (28) (2020) 8519–8525.